

Geophysical Research Letters®

RESEARCH LETTER

10.1029/2024GL111655

Key Points:

- We present a 2-D shear wave velocity model across western Hispaniola Island (Haiti) by joint inversion of Rayleigh wave velocity and H/V
- Our measured H/V ratios, Rayleigh wave velocities, and shear wave velocity model show consistent patterns with the geological units
- The crustal thickness in central Haiti could be thinner than previously estimated from receiver function analysis

Supporting Information:

Supporting Information may be found in the online version of this article.

Correspondence to:

H.-Y. Lee,
hlee423@ucr.edu




Citation:

Lee, H.-Y., Douilly, R., Rabade, S., & Lin, F.-C. (2025). Imaging the deformation belt of western Hispaniola Island (Haiti) using multi-component ambient noise cross-correlations. *Geophysical Research Letters*, 52, e2024GL111655. <https://doi.org/10.1029/2024GL111655>

Received 1 AUG 2024

Accepted 9 DEC 2024

Imaging the Deformation Belt of Western Hispaniola Island (Haiti) Using Multi-Component Ambient Noise Cross-Correlations

Hsin-Yu Lee¹ , Roby Douilly¹, Santiago Rabade² , and Fan-Chi Lin² 

¹Department of Earth and Planetary Sciences, University of California, Riverside, CA, USA, ²Department of Geology and Geophysics, University of Utah, Salt Lake City, UT, USA

Abstract We apply ambient noise tomography to a seismic array from the Trans-Haiti project to obtain a 2-D shear wave velocity (V_s) across Haiti. We perform multi-component noise cross-correlation, measure Rayleigh wave phase velocity and its horizontal-to-vertical amplitude ratio (H/V) between periods of 3–18 s, and jointly invert both measurements into V_s for the crustal structures of Haiti. Both H/V and phase velocity measurements exhibit consistent patterns related to the geologic units. Sedimentary basins—CSE and Plateau Central basins—show higher H/V values, while mountain areas—Massif de la Selle, Chaîne des Matheux, Montagnes Noires and Massif de Nord—exhibit lower H/V. Regarding phase velocity, higher velocities are observed in northern and southern Haiti, likely reflecting the thinner crust compared to the thicker crust showing lower velocities in the central part. While our V_s model is consistent with previous model that suggested thinner crustal thickness in the northern and southern Haiti, with thickening in the center, the Moho interface in the central domain might be shallower than previously thought.

Plain Language Summary Seismic hazards have threatened Hispaniola Island throughout human history, particularly Haiti which has experienced catastrophic earthquakes in recent years. However, the crustal structures responsible for the strong seismic shaking during these large earthquakes remain enigmatic. Therefore, in this study, we utilize ambient noise signals recorded by seismometers to decipher the detailed crustal structures in terms of seismic velocity. The seismic velocity results show that the crustal thickness in the central part of the island might be thinner than previously thought. Additionally, we observe low velocities beneath sedimentary basins, which shows consistent patterns with the geological observations and results from local earthquake tomography. These findings provide valuable and fundamental information for further assessment of seismic hazards in the Haiti area.

1. Introduction

Hispaniola Island sits at a complex boundary in an east-west direction between the North American and Caribbean plates, marking a significant tectonic transition (Figure 1a). To the east, there is a high oblique subduction zone in the region of Puerto Rico (e.g., ten Brink & Lin, 2004), while to the west, a dominantly strike-slip fault system characterizes the south of Cuba (e.g., Calais & de Lepinay, 1991). Located within this transition zone between subduction and transform systems, Hispaniola Island undergoes oblique collision and transpression with a subducted North American slab marked by the down-going seismicity in the eastern region of the island (Figure 1(a)). In contrast, no clear subducted-related seismicity is observed in the central and western regions of the island (e.g., Corbeau et al., 2017; Mann et al., 1995; Sun et al., 2021). Instead, the surface geology shows a series of fold-and-thrust deformation belts with alternating mountain ranges, basins and two major strike-slip fault systems: the Septentrional-Oriente fault (SOF) to the north and the Enriquillo-Plantain Garden fault (EPGF) to the south (Figure 1b). Several major earthquakes struck this island in history (Bakun et al., 2012; ten Brink et al., 2011), including the recent significant events in 2010 and 2021 in southern Haiti. The M7.0 2010 earthquake, with an epicenter less than 25 km from the capital of Haiti (Port-au-Prince), caused more than 200,000 deaths and left more than one million people homeless. It is now clear that this earthquake occurred on a previously unknown structure called the Leogane fault (Calais et al., 2010; Douilly et al., 2013), rather than on the EPGF as initially thought. About a decade later, the M7.2 2021 earthquake, occurred approximately 150 km west of the capital, led to more than 2,200 deaths and is thought to have ruptured on structures adjacent to the EPGF to the north (Douilly et al., 2023). These earthquakes

© 2025. The Author(s).

This is an open access article under the terms of the [Creative Commons Attribution-NonCommercial-NoDerivs License](#), which permits use and distribution in any medium, provided the original work is properly cited, the use is non-commercial and no modifications or adaptations are made.

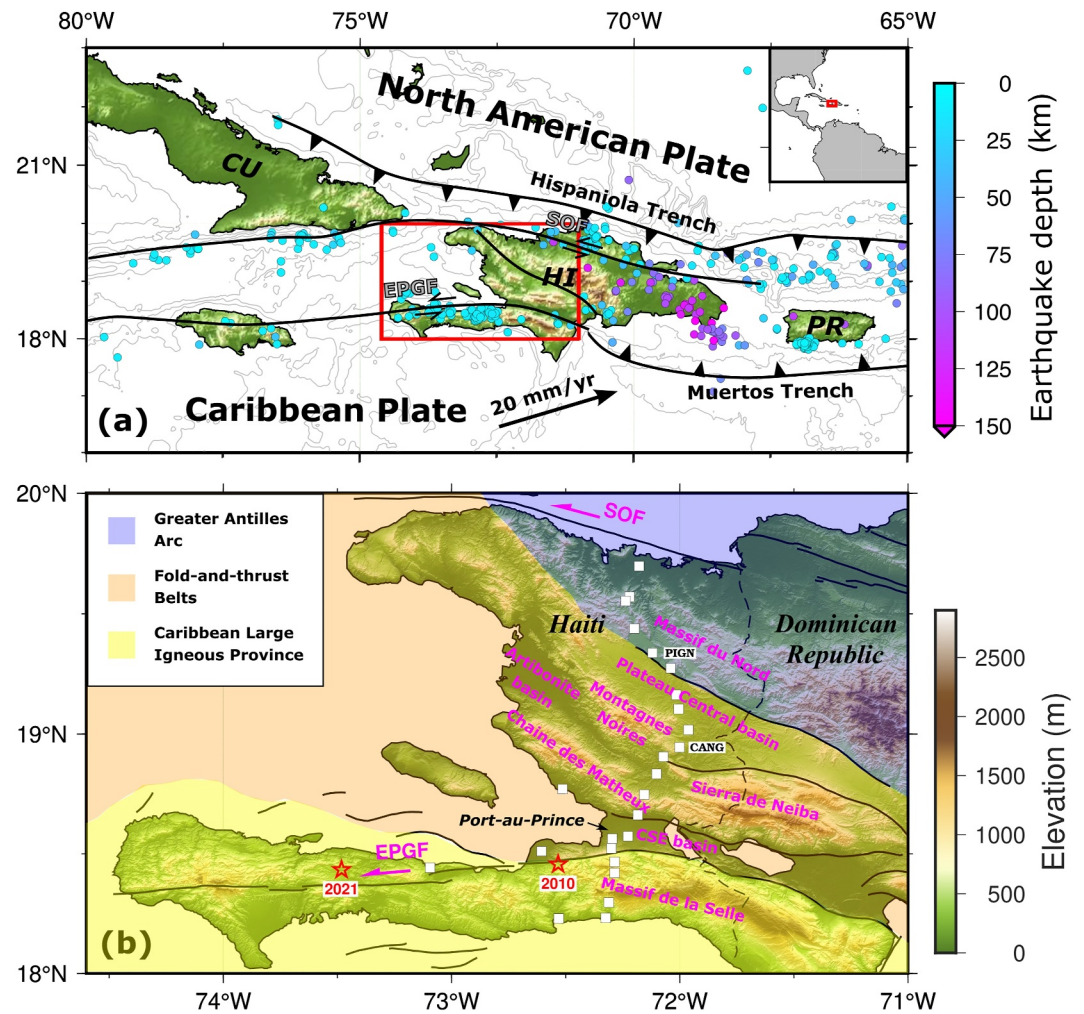


Figure 1. (a) Tectonic setting of plate boundary between the North American plate and Caribbean plate (modified from Núñez et al., 2019). Black arrow indicates the movement of the Caribbean plate with respect to the North American plate. Black lines with triangles delineate trenches. Black lines describe tectonic features. Red rectangle shows the study area for this research. SOF: Septentrional-Oriente fault; EPGF: Enriquillo-Plantain Garden fault; PR: Puerto Rico; CU: Cuba; HI: Hispaniola (comprising Haiti and the Dominican Republic). Blue-purple circles color-coded with depth show the seismicity with magnitude greater than 4.5 in 2000–2024, which is from the ISC-GEM earthquake catalog. (b) Tectonic units in Hispaniola Island. Blue, orange and yellow shades represent the northern, central and southern domains, respectively, which is referred from Corbeau et al. (2017). Seismic stations are represented by white squares. Red stars mark the 2010 and 2021 earthquakes. CSE basin: Cul-de-Sac-Enriquillo basin.

highlight the need for increased vigilance and improved mitigation efforts for future earthquakes in the region.

Following the devastating 2010 earthquake in Haiti, a series of geological and geophysical studies were promptly conducted to investigate the tectonic structures in the region (e.g., Kumar et al., 2023; Possee et al., 2020; Sun et al., 2021). Douilly et al. (2016) utilized the aftershock of the 2010 event to construct a local seismic tomography model in the rupture area. Their findings revealed low seismic velocities in the fault zone and sedimentary basins. Similarly, Possee et al. (2019) used local earthquakes extracted from the 2013–2014 data set to image the crustal structures across Haiti in a north-south direction. A south-dipping fault along the southern border of the Cul-de-Sac-Enriquillo (CSE) basin was shown by a low velocity and high V_p/V_s ratio, which was explained to be a possible extension of the EPGF to the east. Using the same data set, Corbeau et al. (2017) employed receiver function analysis to determine three distinctive crustal domains across Haiti: thinner crust (~ 20 km) in the northern and southern domains (blue and yellow shades in Figure 1b) associated with volcanic arc facies and the

Caribbean Large Igneous Province (CLIP) respectively, while a thicker collisional wedge for the crust (~40 km) in the central part of Haiti (orange shade in Figure 1b). Corbeau et al. (2017) argued that this increase in thickness is due to the CLIP material underthrusting the island arc material in central Haiti. Another explanation that was proposed for the thicker crust in central Haiti is the collapse of a back-arc basin, belonging to the Yucatan Basin, filled with an abundance of volcanic rock fragments (Ramos & Mann, 2023). Regional tomographic imaging of the Caribbean area conducted by Quiros et al. (2018) & Moreno Toiran et al. (2023) highlighted variations in seismic velocities across different terranes, suggesting variations in crustal thickness across the region. The crustal thickness was reported as ~5 km thick offshore southern Haiti, 20–30 km in the Beata Ridge (Mauffret & Leroy, 1999), ~15 km in the center of the Caribbean plate (Leroy et al., 2000), ~20 km for the CLIP (e.g., Calais et al., 2023), and ~30 km in the central Hispaniola underneath the Dominican Republic (Kumar et al., 2020; Núñez et al., 2019; Sun et al., 2021).

Despite these advancements, the resolution of existing studies remains limited, particularly in the crustal structure. Receiver function analysis is constrained by its sensitivity to structural discontinuities beneath stations, while local earthquake tomography is restricted by earthquake observations, in which earthquake detection in this region has been shown to be a challenging task (e.g., Lee & Douilly, 2023). To address these limitations, ambient noise tomography has emerged as a valuable tool, offering improved resolution for shallow crustal structures through joint inversion of Rayleigh wave velocities and its horizontal-to-vertical amplitude ratio (H/V), as demonstrated by Berg et al. (2018), Liu et al. (2021) & Rabade et al. (2023). The detailed structures hold significant implications for simulation-based seismic hazard studies, particularly in densely populated areas.

Therefore, in this study, we investigate the crustal structure across Haiti by applying ambient noise tomography. We perform multi-component noise cross-correlation and measure Rayleigh wave phase velocity and H/V ratio mainly from the 2013–2014 data set, consisting of 24 broadband stations deployed across the Haiti area. We then jointly invert both phase velocity and H/V ratio for a 2-D profile shear wave velocity (V_s) model of Haiti.

2. Data and Methods

2.1. Data and Ambient Noise Cross-Correlation

The data used in this study are mainly from 24 broadband stations as part of the Trans-Haiti project deployed from April 2013 to June 2014 (Figure 1b). Most stations were deployed along a north-south transect across the deformation belt of western Hispaniola with an average spacing of approximately 10 km (Corbeau et al., 2017). For each station and each component, we first remove the mean, trend and instrument response from the daily time series recordings. We then apply temporal normalization and spectral whitening simultaneously to the three-component data prior to cross correlation, following the method described by Bensen et al. (2007) and Lin et al. (2014). We next cross-correlate all available three-component seismograms between all stations, stack the daily cross-correlation functions (CCFs), and rotate the horizontal components (E-W and N-S components) into radial and transverse components, following the methods of Lin et al. (2008). Next, we sum the positive and negative components of each cross-correlation to improve the signal-to-noise ratio (SNR) (e.g., Wang et al., 2017). Finally, we calculate the H/V amplitude ratios and Rayleigh wave phase velocities from ZZ, ZR, RZ, and RR components (Z and R represent vertical and radial components, respectively). Figure 2a shows an example of the ZZ symmetric component cross-correlations with a bandpass filter 3–18 s for the station pairs in the Haiti area. The ZR, RZ, and RR component cross-correlations can be found in Figure S1 in Supporting Information S1. Clear Rayleigh wave signals are observed in all four components. We did not calculate the H/V ratios for stations STRA, CAYH, THOM and MIRB due to incorrect amplitude recordings or malfunction at these stations' horizontal components (e.g., Figure S2 in Supporting Information S1).

2.2. Rayleigh Wave Ellipticity and Phase Velocity

We apply frequency-time analysis (FTAN; Bensen et al., 2007) to determine Rayleigh wave traveltimes and amplitudes in the ZZ, ZR, RZ and RR component cross-correlations between the periods of 3–18 s. Assuming a diffusive noise wavefield, the ZZ, ZR, RZ and RR cross-correlations can be related to the Rayleigh wave Green's functions where the two letters denote the force and receiver directions at the first and second stations, respectively (Lin et al., 2014). Hence, the combination of ZZ and ZR or RZ and RR cross-correlations allows us to study the Rayleigh wave elliptical particle motion at the receiver station. Conversely, following the reciprocity principle, the combination of ZZ and RZ or ZR and RR cross-correlations can be used to study the particle motion at

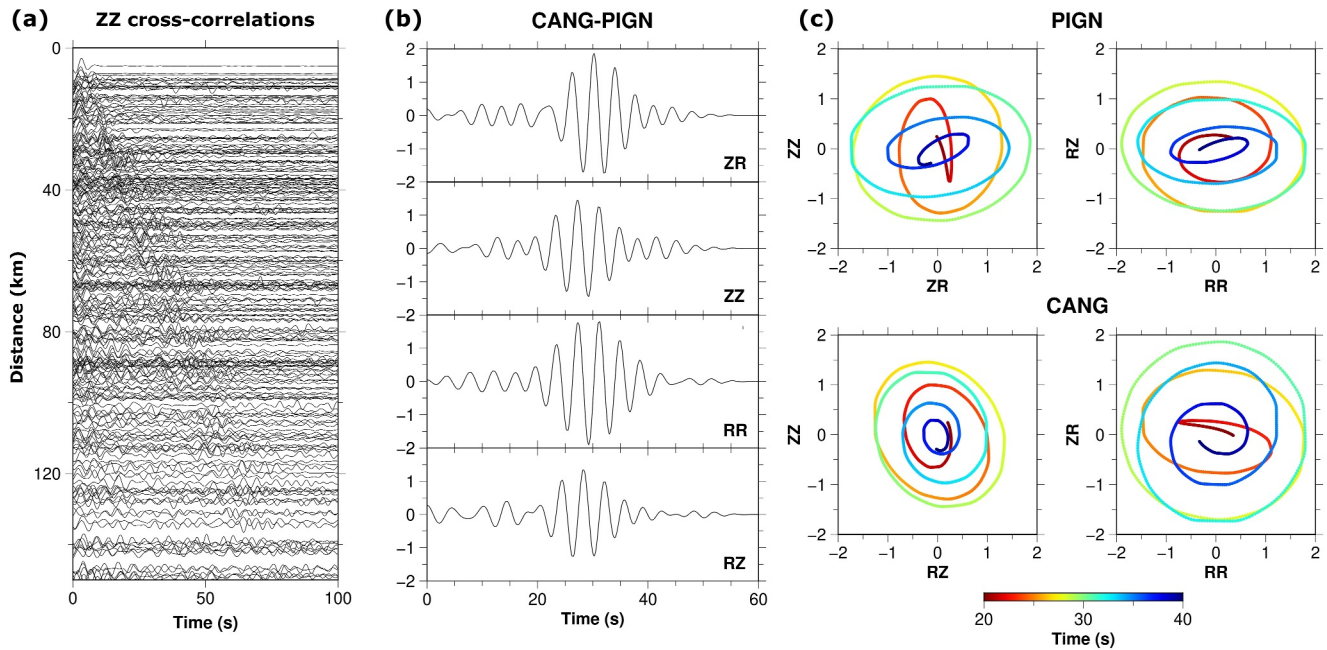


Figure 2. (a) Noise cross-correlations with a bandpass filter 3–18 s from the ZZ (vertical-vertical) component of the station pairs in the Haiti area. (b) Four component (ZR, ZZ, RR and RZ) noise cross-correlations between stations CANG and PIGN with a bandpass filter around 4 s. (c) Rayleigh wave particle motions for the waveforms in (b). Top panel: the particle motion at station PIGN. Bottom panel: the particle motion at CANG.

the source station. We use all available virtual sources (Z or R) to determine the H/V ratio at virtual receiver stations. We set several selection criteria to retain reliable H/V values including removing the measurements with SNR smaller than 5, interstation distance smaller than 2 wavelengths, and the measurements greater than 2 standard deviations of all data. The representative H/V ratio at a station is calculated by the average of the selected H/V measurements of the station. Figure 2b shows an example of the ZZ, ZR, RZ and RR component cross-correlations between stations CANG and PIGN (Figure 1b) with a bandpass filter near 4 s. The observations of the maximum amplitude on the four components are different. The different H/V ratios between CANG and PIGN can be seen from the particle motions in Figure 2c, in which PIGN located in the basin has a higher H/V ratio whereas CANG in the mountain area has a lower H/V.

Similarly, we set the same criteria for phase traveltime measurements, including removing the measurements with SNR smaller than 5 and interstation distance smaller than 2 wavelengths. We correct the $\pm 90^\circ$ phase shifts for RZ and ZR components compared to ZZ and RR and apply 2π jump correction for all four components prior to extracting the reliable measurements (e.g., Lin et al., 2008; Wang et al., 2017). Figures 3a–3c show the phase velocity measurements and ray coverage map for the ZZ components at 4, 8 and 12 s. With these selected measurements, we invert for a 2-D Rayleigh wave phase velocity map in a 0.1×0.1 grid size using the 2-D tomographic method of Barmin et al. (2001). We remove all measurements with residuals greater than 2 standard deviations in the initial inversion and derive the final phase velocity maps (Figures 3g–3i) in the subsequent inversion.

2.3. MCMC Joint Inversion

We jointly invert Rayleigh wave phase velocity and H/V ratio for a 1-D Vs at each station site by using the Markov Chain Monte Carlo (MCMC) method (e.g., Berg et al., 2020; Liu et al., 2021; Shapiro & Ritzwoller, 2002). The phase velocities at each station are extracted from the results of the 2-D velocity maps, and we assign an uncertainty of 0.1 km/s for the phase velocity measurements, using estimates from previous studies of a similar nature (e.g., Paul et al., 2024; Yang et al., 2011). The sensitivity kernels of the Rayleigh wave phase velocities and H/V ratios at 3–18 s allow the crustal structure to be resolved from the surface to ~ 40 km depth (Figure S3 in Supporting Information S1). We use the 1-D Vs model from Possee et al. (2019) as a starting reference model and determine Vp and density structure from the empirical relations described in Brocher (2005). The initial model is

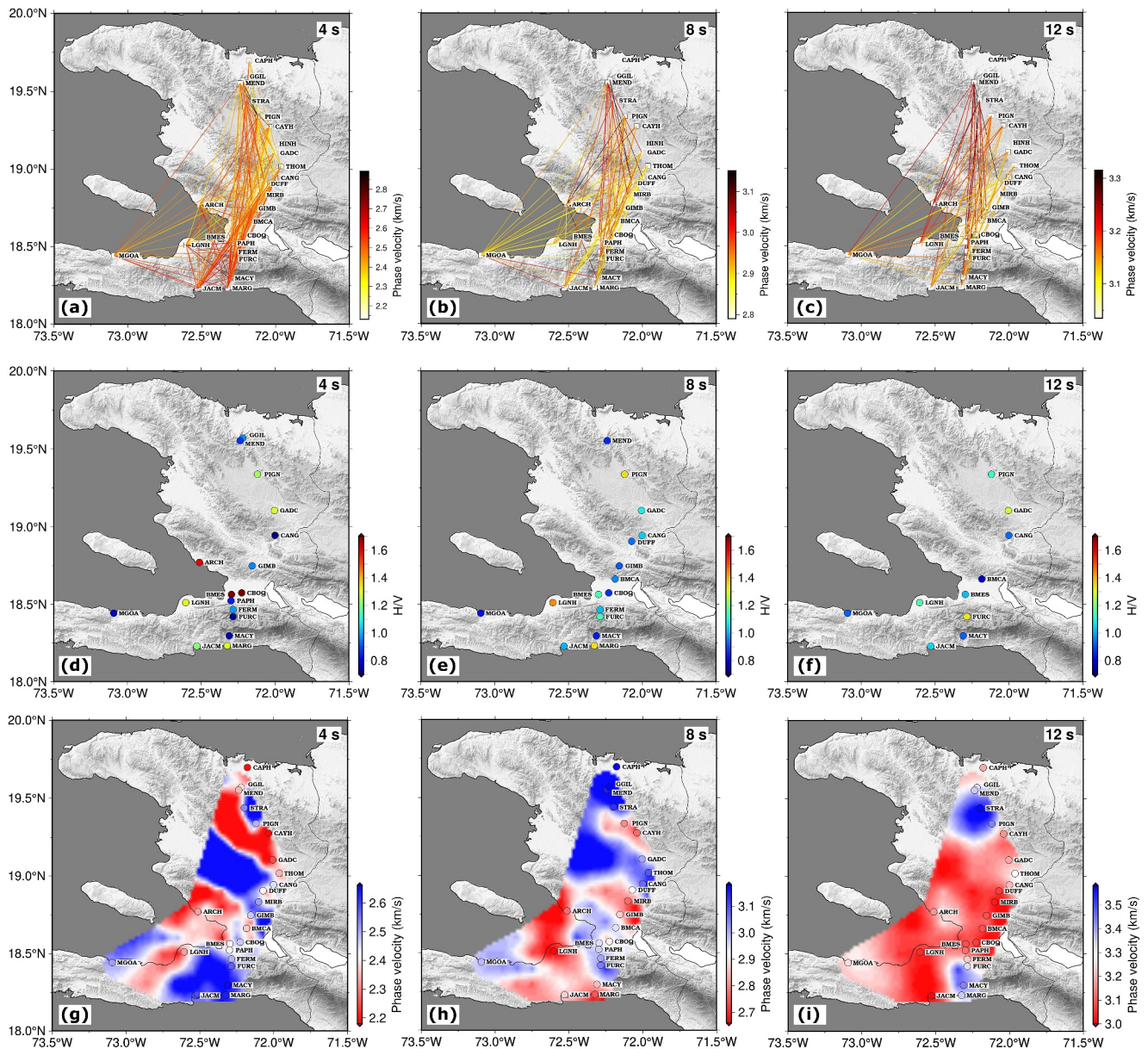


Figure 3. (a) Phase velocity measurements and ray coverage map at 4 s. (c)–(d) Same as (a) but for 8 and 12 s. (d) Rayleigh wave H/V measurements across Haiti at 4 s. (e)–(f) Same as (d) but for 8 and 12 s. (g) Rayleigh wave phase velocities across Haiti at 4 (h)–(i) Same as (g) but for 8 and 12 s.

parameterized with a linearly increasing sedimentary layer (0–4 km depth) and the rest of the crust (4–40 km depth) described by 5 cubic B-splines. During the inversion, the thickness of the sedimentary layer is flexible, and we allow to change the boundary depth between sediment and crust. Following the setup by Rabade et al. (2023), we allow the MCMC inversion to search for V_s that are up to ± 1.5 and ± 3 km/s for the sedimentary layer and the rest of the crust, respectively, from the reference model. Besides, two constraints are imposed: (a) we allow a maximum V_s of 5 km/s in the crust, and (b) consider a positive velocity jump at the base of the sedimentary layer. For each inversion, we compute 3,000 randomly generated iterations with 6 jumps, and only accept the models within 1.5 times the minimum misfit. The final V_s velocity model is constructed from the average of all the accepted models. Figure S4 in Supporting Information S1 shows an example of MCMC joint inversion for a 1-D V_s at station BMES, which is located in the CSE basin.

3. Results

Figure 3d illustrates the H/V ratios measured at each station site at 4 s, where H/V is most sensitive to shallow crustal structures (above ~5 km depth; Figure S3 in Supporting Information S1). The results exhibit significant variation across Haiti, consistent with the geological units documented in previous studies (e.g., Escuder Viruete et al., 2006; Mann et al., 1995; Saint Fleur et al., 2019). High H/V ratio areas are correlated with major sedimentary basins such as the CSE basin and Plateau Central basin, as well as coastal regions, in contrast, lower H/V ratios are observed in mountain areas like Massif du Nord, Montagnes Noires, Chaîne des Matheux, and Massif de la Selle. We should note that the highest H/V values at 4 s recorded at stations BMES (2.41) and CBOQ (2.35) in the CSE basin, where the capital of Haiti is located and was heavily hit by the 2010 earthquake. In contrast, the lowest values are found at stations CANG (0.69) in the Montagnes Noires, and FURC (0.72) and MACY (0.75) in the Massif de la Selle in southern Haiti. At longer periods (8 and 12 s) (Figures 3e and 3f), H/V ratios show less variation across the array, with predominantly lower values (below 1.4). Notably, H/V ratios decrease to below 1.2 in the CSE basin for both stations (BMES and CBOQ) at 8 s. Combined with the observations of H/V at 4 s, these results suggest a velocity contrast between the shallow layer (above 1 km depth) and the underlying structural layer. Additionally, station LGNH, situated near the Leogane fault responsible for the 2010 event, exhibits a higher H/V value at 8 s compared to 4 s, possibly indicating that the fault and its associated damage zone are buried below the uppermost crust, consistent with the seismic activity from Douilly et al. (2013) and the low-velocity zone shown in Douilly et al. (2016).

In our phase velocity analysis, we observe a general trend of increasing velocities with longer periods (Figures 3g–3i). At 4 s (Figure 3g), Rayleigh wave phase velocity is most sensitive to depths of approximately 3–8 km (Figure S3 in Supporting Information S1). We note the correlations between phase velocities and geological features, including lower velocities in the Plateau Central basin and higher velocities in the Massif de la Selle. As we extend to longer periods (e.g., 12 s; Figure 3i), which are most sensitive to depths of approximately 10–15 km, our result reflects the pattern of mid-crust/lower crust characteristics that is consistent with previously defined three structural features (Corbeau et al., 2017). Specifically, we observe higher velocities in the northern and southern regions of Haiti, contrasting with lower velocities in the central portion, corresponding to the thicker crust of the fold-and-thrust belt.

Figure 4 presents the 2-D profile of the V_s model across Haiti, which is interpolated using the minimum curvature solution from the 1-D V_s result at each station. Contrary to the 2D velocity model from Possee et al. (2019), our 2-D V_s model reveals distinct crustal structures in northern, central, and southern Haiti, corresponding to the Greater Antilles Arc (GAA), fold-and-thrust belt, and CLIP, respectively. To guide the discussion, we use V_s values of 3.3 km/s (orange to yellow in Figure 4) and 3.6 km/s (yellow to green in Figure 4) to roughly delineate upper, middle, and lower crust. Our V_s model shows upper crust extending to depths of 10–15 km beneath the CSE, Artibonite, and Plateau Central basins, suggesting the presence of thicker sedimentary structure beneath these basins. Additionally, in middle crust, we observe a south-dipping fold structure beneath stations PAPH and FREM (southern CSE boundary) and a north-dipping fold structure beneath stations CAYH and PIGN (northern Plateau Central boundary). These structures (dashed purple lines in Figure 4) are aligned with the large-scale deformation patterns identified in the geological observations from Mann et al. (1991). These tilting structures and verging folds at the boundaries of the CSE and Plateau Central basins suggest that the thick sedimentary basins were formed by being pushed down along thrusts from both sides due to compressional stress, which led to large, sediment trap and depocenters (see Figure 6 from Mann et al. (1991)). These observed structures are also consistent with the oblique low V_p and high V_p/V_s anomalies from Possee et al. (2019). Furthermore, the Moho interface (the black line and black dashed line in Figure 4), defined as the contour line with a V_s of 4 km/s (Moreno Toiran et al., 2023), also depicts different crustal structures in northern, central, and southern Haiti. We observe that the Moho interface is located at an average depth of 22 km for the southern domain, 24–32 km for the central domain, and possibly ~15 or 20–25 km for northern Haiti. This will be further discussed in Section 4.

To assess the stability of the joint inversion from the measurements, Figure S5 in Supporting Information S1 illustrates the observed Rayleigh wave phase velocity and H/V, which are used as inputs for the shear wave velocity inversion, along with the corresponding normalized misfits between the observations and the final resolved models. The results indicate that phase velocities demonstrate greater stability compared to H/V, providing more reliable constraints on crustal structures deeper than ~5 km. In contrast, H/V measurements exhibit relative instability, particularly noticeable at shorter periods in the central and northern island. This could

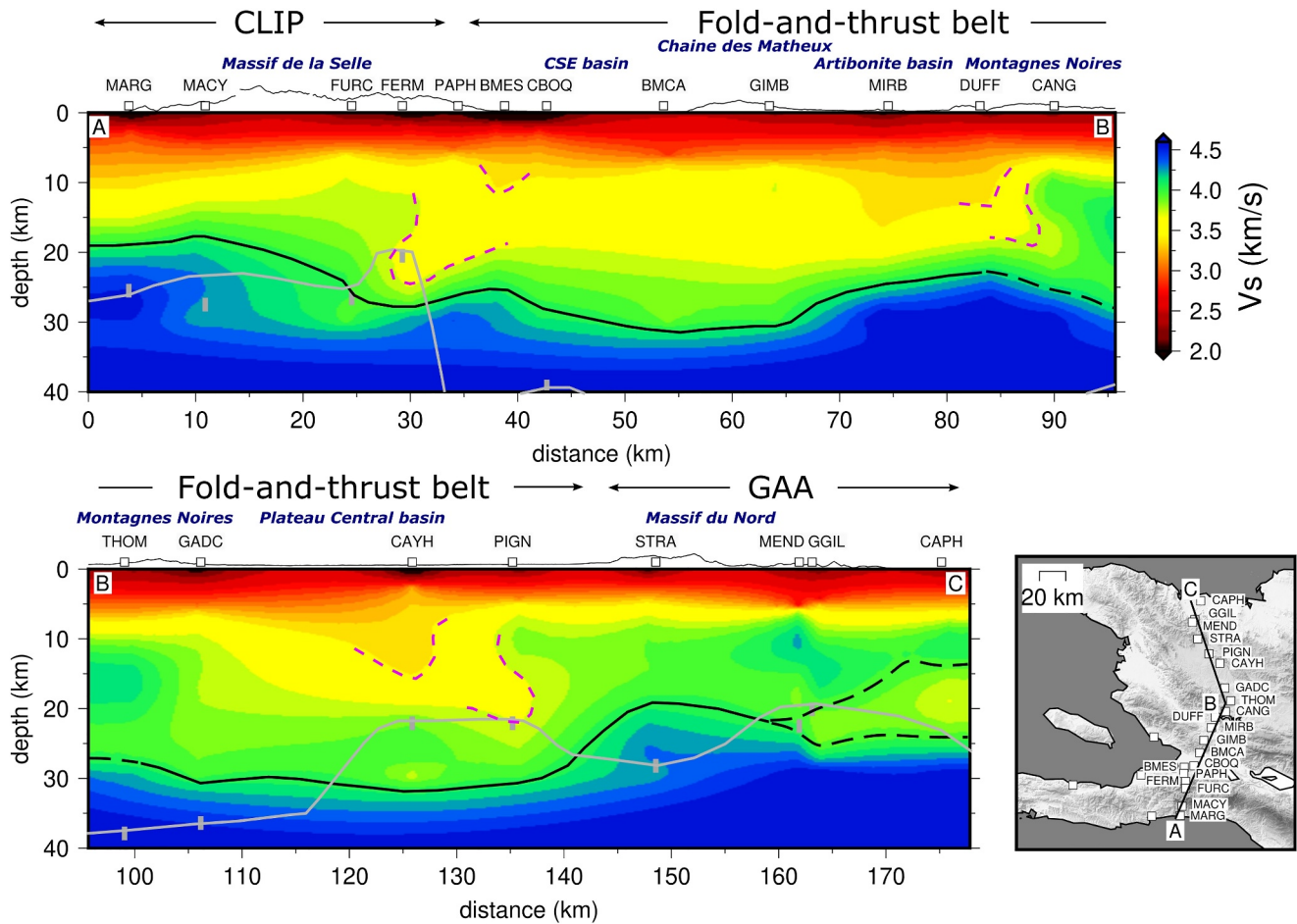


Figure 4. 2-D cross-sections of the final inversion shear wave velocity (V_s) model across Haiti. The location of the cross-sections is identified in the bottom right panel. Top panel: cross-section A-B, from the south of Haiti to the central part. Bottom left panel: cross-section B-C, from the central part of Haiti to the north. Stations are marked with white squares along the cross-sections. The black line marks the Moho interface defined as 4.0 km/s in the study. The black dashed line is used for locations where there are multiple depths with 4.0 km/s V_s . Gray bars are the Moho depth defined from receiver function by Corbeau et al. (2017). Gray lines are the Moho depth from the gravity model by Sun et al. (2021) which used Corbeau et al. (2017) as constraints. Purple dashed lines mark the folding structures mentioned in the main text.

be due to the fact that H/V ratios are mostly sensitive to structures directly beneath the stations. Thus, shallow small-scale heterogeneity at station sites might cause instability. Additionally, as we mentioned in Section 2.1, we did not incorporate the H/V measurements from stations STRA, CAYH, THOM, and MIRB into the results due to incorrect amplitude recordings (one example is shown in Figure S2 in Supporting Information S1). However, we decided it is still worthwhile to include the H/V measurements where they are available to provide constraints on the shallow crust.

4. Discussion

The variation in crustal thickness in the central part of Hispaniola Island has been debated based on two main competing crustal interpretations. Corbeau et al. (2017) conducted a receiver function analysis and proposed, combined with geological evidence, that the Moho depth abruptly increases from approximately 23 km in the north and south to about 41 km in the central portion of Haiti. Additionally, Sun et al. (2021) used several north-south 2-D gravity transects to constrain the crustal structure across the island. In western Hispaniola (Haiti), using the results from Corbeau et al. (2017) as constraints for crustal structures, their transect 1 suggested that the central region has a Moho depth of about 40 km, which supported the model of Corbeau et al. (2017). However, their adjacent transect 2 in the Dominican Republic showed that the Moho depth in the central region is about 6 km shallower which is in agreement with the Moho depth from the seismic reflection and refraction analysis from Núñez et al. (2019) and the receiver function analysis from Kumar et al. (2020). This shallower Moho depth

(~30 km) in the central part of the island is conserved even further east of the island (transect 3 from Sun et al. (2021)). Considering how uniform (~30 km) the Moho depth is in the central region underneath the Dominican Republic (Kumar et al., 2020, 2023; Núñez et al., 2019; Sun et al., 2021), it is worth investigating whether the Moho depth in the central region underneath Haiti is in agreement with the one underneath the Dominican Republic or whether it is much thicker (~40 km). To revisit this debated topic of crustal thickness variation from north to south across the island, we provide an independent result from ambient noise tomography, which has been widely used in investigating crustal structure (e.g., Karplus et al., 2013; Movaghari & Doloei, 2020; Ward, 2015). While the variation in crustal thickness in the central part of the island remains elusive, it is important to emphasize that all the available models are in agreement that the Hispaniola island has a thinner crustal thickness of about 22–25 km in the northern and southern parts of the island, with thickening in the center.

Focusing on Moho depth, we relate our shear wave velocity model to the crustal models proposed by Corbeau et al. (2017) and Sun et al. (2021) in the northern, southern, and central domains of Haiti, corresponding to GAA, fold-and-thrust belt, and CLIP respectively (Figure 4). We define the Moho interface as the depth of the 4.0 km/s velocity contour in our model, which reflects ultramafic materials in deeper crust (e.g., Paul et al., 2024) and is consistent with the knowledge of the study area (e.g., Moreno Toiran et al., 2023; Núñez et al., 2019). The solid black lines and the dashed black lines in Figure 4 delineate our interpretation of the Moho interface across Haiti in the N-S direction.

Previous studies have interpreted the southern domain as part of the CLIP, consisting of significant basalt formations formed during the Cretaceous period on the Pacific Farallon plate (Duncan & Hargraves, 1984). Our Vs model at stations MARG and MACY shows the crustal thickness is ~20 km, which is about 6 km shallower than the observation from the receiver function (depicted with the gray bar in Figure 4). Further north in the southern domain, our results at station FURC show agreement with Corbeau et al. (2017), where the Moho depth is ~26 km. On average, our shear wave velocity model shows that the crustal thickness is 22 km for the southern domain, consistent with both previously proposed models. However, at station PAPH, located at the boundary between the southern and central domains defined by Corbeau et al. (2017), we do not observe a deep Moho depth (~42 km) as shown in the receiver function results; instead, it is ~26 km in our results. While we do not observe the Moho depth reaching 40 km, a thick layer with Vs of 3.5 km/s is present beneath station PAPH, indicating a possible different tectonic structure beneath PAPH compared to the southern domain.

The central part of Haiti comprises a collisional wedge characterized by fold-and-thrust deformation belts with alternating mountain ranges and basins, originating from the early Miocene (Pubellier et al., 1991). As the previous two models suggested, our Vs model shows a deeper Moho depth in the fold-and-thrust belt compared to the south, implying crustal thickening in the area (e.g., Corbeau et al., 2017; Sun et al., 2021). However, compared to both Corbeau et al. (2017) and Sun et al. (2021), our Vs model indicates a shallower Moho interface, ranging from 24 to 32 km in the central domain, which is ~10 km shallower than their model. In the southern fold-and-thrust belt, the Moho interface defined by Corbeau et al. (2017) is deeper than 40 km, which is beyond our result resolution. Further north of the fold-and-thrust belt, at stations THOM and GADC, a ~30 km Moho depth from our model is more consistent with Corbeau et al. (2017) and Sun et al. (2021). In general, our model in the central portion is in agreement with the crustal thickness in the Dominican Republic, which has an average Moho depth of 30 km. It is worth noting in our study that the boundary between the central and northern domains may be located around station PIGN or between stations PIGN and STRA since the Moho depth significantly changes at that location, instead of around CAYH as Corbeau et al. (2017) proposed.

The GAA in the northern domain corresponds to the Cretaceous volcanic arc, primarily composed of arc magmatic facies (Escuder Viruete et al., 2006; Pindell et al., 2006). Our Vs model shows the Moho interface beneath station STRA is ~20.8 km shallower than Corbeau et al. (2017). Further north, stations MEND and GGIL show consistent Moho observations with Corbeau et al. (2017). We conclude that our Vs model is consistent with both models, showing a ~20 km Moho depth in the northern domain. However, our Vs model shows a poor inversion recovery between model and observation data (Figure S5 in Supporting Information S1 left bottom panel at 12–16 periods) toward further north. Thus, we propose two possible options for the Moho interfaces (black dashed line in Figure 4). One is that the Moho interface gradually decreases to ~15 km toward the north, while the other suggests the Moho interface stays between 20 and 25 km toward the north. Future studies with a

denser network that could lead to a higher resolution should be considered to clarify the true Moho configuration at that location.

While we use the same stations during the same time period as Corbeau et al. (2017), our observed Moho at certain stations, particularly in the central crust of Haiti, differ from theirs. This discrepancy may arise from using different seismic sources, seismic phases and tomography techniques. Corbeau et al. (2017) relied on teleseismic sources focused on P-phase conversions, which are sensitive to contrasts directly beneath the stations. In contrast, we use ambient noise sources from the region, focusing on Rayleigh waves, and define the Moho interface based on the reference Vs in the region (Moreno Toiran et al., 2023; Núñez et al., 2019; Possee et al., 2019). Furthermore, it is important to emphasize that Sun et al. (2021) used the results from Corbeau et al. (2017) to constrain the crustal depth in their transect 1. Therefore, without this added constraint, it is possible that the crustal thickness in transect 1 could be more in line with their transects 2 and 3 and thus with our crustal interpretation.

Our 2-D cross-section Vs model provides insights into the crustal structure across western Hispaniola Island, offering essential parameters for further applications in seismic hazard assessment, such as earthquake location and ground motion simulation. This is paramount for this area, which has experienced several major earthquakes in history, including the recent 2010 and 2021 Haiti earthquakes. In the future, we expect to construct a 3-D high-resolution velocity map in this area, which will require the investment of significant resources.

5. Conclusions

We perform multi-component noise cross-correlation and measure Rayleigh wave phase velocity and its horizontal-to-vertical amplitude ratio (H/V) across Haiti. The H/V and phase velocity results show consistent patterns related to the geologic units. At short periods, the sedimentary basins and areas near the coast exhibit higher H/V values, while the mountain areas show lower H/V. At longer periods, H/V ratios show less variation across the array, with predominantly lower values. Regarding phase velocity, at longer periods, which reflect the mid-crust/lower crust characteristics, we observe higher velocities in northern and southern Haiti and lower velocities in the central portion. We also conduct a joint inversion of H/V and phase velocity to construct a 2-D Vs model across Haiti and define the Moho interface as the depth of the 4.0 km/s velocity contour in our model. While our Vs model is consistent with previously proposed models that suggested thinner crustal thickness in northern and southern Haiti with thickening in the center, the Moho interface in the central domain might be shallower than previously thought. While this study provides a better understanding of the crustal structure across Haiti, additional future investigations on a 3-D high-resolution velocity map are needed. This will require more broadband stations or a dense nodal array to provide better data coverage and quality.

Data Availability Statement

The seismic data from Trans-Haiti project can be accessed through EarthScope Data Center (IRIS DMC) at: https://www.fdsn.org/networks/detail/ZU_2013/.

References

- Bakun, W. H., Flores, C. H., & ten Brink, U. S. (2012). Significant earthquakes on the Enriquillo fault system, Hispaniola, 1500–2010: Implications for seismic hazard. *Bulletin of the Seismological Society of America*, 102(1), 18–30. <https://doi.org/10.1785/0120110077>
- Barmin, M. P., Ritzwoller, M. H., & Levshin, A. L. (2001). A fast and reliable method for surface wave tomography. *Monitoring the comprehensive nuclear-test-ban treaty: Surface waves*, 1351–1375. https://doi.org/10.1007/978-3-0348-8264-4_3
- Bensen, G. D., Ritzwoller, M. H., Barmin, M. P., Levshin, A. L., Lin, F., Moschetti, M. P., et al. (2007). Processing seismic ambient noise data to obtain reliable broad-band surface wave dispersion measurements. *Geophysical Journal International*, 169(3), 1239–1260. <https://doi.org/10.1111/j.1365-246x.2007.03374.x>
- Berg, E. M., Lin, F. C., Allam, A., Qiu, H., Shen, W., & Ben-Zion, Y. (2018). Tomography of Southern California via Bayesian joint inversion of Rayleigh wave ellipticity and phase velocity from ambient noise cross-correlations. *Journal of Geophysical Research: Solid Earth*, 123(11), 9933–9949. <https://doi.org/10.1029/2018jb016269>
- Berg, E. M., Lin, F. C., Allam, A., Schulte-Pelkum, V., Ward, K. M., & Shen, W. (2020). Shear velocity model of Alaska via joint inversion of Rayleigh wave ellipticity, phase velocities, and receiver functions across the Alaska Transportable Array. *Journal of Geophysical Research: Solid Earth*, 125(2), e2019JB018582. <https://doi.org/10.1029/2019jb018582>
- Brocher, T. M. (2005). Empirical relations between elastic wavespeeds and density in the Earth's crust. *Bulletin of the Seismological Society of America*, 95(6), 2081–2092. <https://doi.org/10.1785/0120050077>
- Calais, E., & de Lepinay, B. M. (1991). From tension to transpression along the northern Caribbean plate boundary off Cuba: Implications for the recent motion of the Caribbean plate. *Tectonophysics*, 186(3–4), 329–350. [https://doi.org/10.1016/0040-1951\(91\)90367-2](https://doi.org/10.1016/0040-1951(91)90367-2)
- Calais, E., Freed, A., Mattioli, G., Amelung, F., Jónsson, S., Jansma, P., et al. (2010). Transpressional rupture of an unmapped fault during the 2010 Haiti earthquake. *Nature Geoscience*, 3(11), 794–799. <https://doi.org/10.1038/ngeo992>

Acknowledgments

We thank Françoise Courboux and Anne Deschamps for sharing the seismic data and Jyun-Nai Wu for the helpful feedback on this article. The authors are grateful to the two anonymous reviewers for their thoughtful and constructive feedback which has greatly improved this manuscript. The figures in the study are plotted with Generic Mapping Tools 6 (Wessel et al., 2019). This research is supported by the startup fund of Roby Douilly, the NSF grant (award number EAR-2217976) of Roby Douilly and the NSF grant (award number EAR-1753362) of Fan-Chi Lin.

- Calais, E., Symithe, S. J., & de Lépinay, B. M. (2023). Strain partitioning within the Caribbean–North America transform plate boundary in southern Haiti, tectonic and hazard implications. *Bulletin of the Seismological Society of America*, *113*(1), 131–142. <https://doi.org/10.1785/0120220121>
- Corbeau, J., Rolandone, F., Leroy, S., Guerrier, K., Keir, D., Stuart, G., et al. (2017). Crustal structure of western Hispaniola (Haiti) from a teleseismic receiver function study. *Tectonophysics*, *709*, 9–19. <https://doi.org/10.1016/j.tecto.2017.04.029>
- Douilly, R., Ellsworth, W. L., Kissling, E., Freed, A. M., Deschamps, A., & Mercier de Lépinay, B. (2016). 3-D velocity structure in southern Haiti from local earthquake tomography. *Journal of Geophysical Research: Solid Earth*, *121*(12), 8813–8832. <https://doi.org/10.1002/2016jb013123>
- Douilly, R., Haase, J. S., Ellsworth, W. L., Bouin, M. P., Calais, E., Symithe, S. J., et al. (2013). Crustal structure and fault geometry of the 2010 Haiti earthquake from temporary seismometer deployments. *Bulletin of the Seismological Society of America*, *103*(4), 2305–2325. <https://doi.org/10.1785/0120120303>
- Douilly, R., Paul, S., Monfret, T., Deschamps, A., Ambrois, D., Symithe, S. J., et al. (2023). Rupture segmentation of the 14 August 2021 Mw 7.2 Nippes, Haiti, earthquake using aftershock relocation from a local seismic deployment. *Bulletin of the Seismological Society of America*, *113*(1), 58–72. <https://doi.org/10.1785/0120220128>
- Duncan, R. A., & Hargraves, R. B. (1984). Plate tectonic evolution of the Caribbean region in the mantle reference frame. *Geological Society of America Memoir*, *162*, 81–94. <https://doi.org/10.1130/mem162-p81>
- Escuder Viruete, J., Contreras, F., Stein, G., Urien, P., Joubert, M., Ullrich, T., et al. (2006). Transpression and strain partitioning in the Caribbean Island-arc: Fabric development, kinematics and Ar–Ar ages of syntectonic emplacement of the Loma de Cabrera batholith, Dominican Republic. *Journal of Structural Geology*, *28*(8), 1496–1519. <https://doi.org/10.1016/j.jsg.2006.04.003>
- Karplus, M. S., Klempner, S. L., Lawrence, J. F., Zhao, W., Mechie, J., Tilmann, F., et al. (2013). Ambient-noise tomography of north Tibet limits geological terrane signature to upper-middle crust. *Geophysical Research Letters*, *40*(5), 808–813. <https://doi.org/10.1002/grl.50202>
- Kumar, S., Agrawal, M., & Pulliam, J. (2023). Modeling seismic anisotropy beneath the Island of Hispaniola via the harmonic decomposition of receiver functions. *Geochemistry, Geophysics, Geosystems*, *24*(5), e2022GC010773. <https://doi.org/10.1029/2022gc010773>
- Kumar, S., Agrawal, M., Pulliam, J., Rivera, E. P., & Huérfano, V. A. (2020). Crustal thickness and bulk Poisson ratios in the Dominican Republic from receiver function analysis. *Tectonophysics*, *775*, 228308. <https://doi.org/10.1016/j.tecto.2019.228308>
- Lee, H. Y., & Douilly, R. (2023). Earthquake swarms in southern Hispaniola revealed by spatiotemporal evolution of seismicity from multi-station template matching. *Bulletin of the Seismological Society of America*, *113*(1), 115–130. <https://doi.org/10.1785/0120220125>
- Leroy, S., Mauffret, A., Patriat, P., & Mercier de Lépinay, B. (2000). An alternative interpretation of the Cayman trough evolution from a re-identification of magnetic anomalies. *Geophysical Journal International*, *141*(3), 539–557. <https://doi.org/10.1046/j.1365-246x.2000.00059.x>
- Lin, F. C., Moschetti, M. P., & Ritzwoller, M. H. (2008). Surface wave tomography of the western United States from ambient seismic noise: Rayleigh and love wave phase velocity maps. *Geophysical Journal International*, *173*(1), 281–298. <https://doi.org/10.1111/j.1365-246x.2008.03720.x>
- Lin, F. C., Tsai, V. C., & Schmandt, B. (2014). 3-D crustal structure of the western United States: Application of Rayleigh-wave ellipticity extracted from noise cross-correlations. *Geophysical Journal International*, *198*(2), 656–670. <https://doi.org/10.1093/gji/ggu160>
- Liu, C. N., Lin, F. C., Huang, H. H., Wang, Y., Berg, E. M., & Lin, C. H. (2021). High-resolution 3-D shear wave velocity model of northern Taiwan via Bayesian joint inversion of Rayleigh wave ellipticity and phase velocity with Formosa array. *Journal of Geophysical Research: Solid Earth*, *126*(5), e2020JB021610. <https://doi.org/10.1029/2020jb021610>
- Mann, P., Draper, G., & Lewis, J. F. (1991). An overview of the geologic and tectonic development of Hispaniola. *Geological Society of America Special Paper*, 1–28. <https://doi.org/10.1130/spe262-p1>
- Mann, P., Taylor, F. W., Edwards, R. L., & Ku, T. L. (1995). Actively evolving microplate formation by oblique collision and sideways motion along strike-slip faults: An example from the northeastern Caribbean plate margin. *Tectonophysics*, *246*(1–3), 1–69. [https://doi.org/10.1016/0040-1951\(94\)00268-e](https://doi.org/10.1016/0040-1951(94)00268-e)
- Mauffret, A., & Leroy, S. (1999). Neogene intraplate deformation of the Caribbean plate at the Beata Ridge. *Sedimentary basins of the world*, *4*, 627–669.
- Moreno Toiran, B., Aoudia, A., Manu-Marfo, D., Kherouchou, R., & Pachhai, S. (2023). Crust–uppermost mantle structure beneath the Caribbean region from seismic ambient noise tomography. *Bulletin of the Seismological Society of America*, *113*(3), 1064–1076. <https://doi.org/10.1785/0120220062>
- Movaghari, R., & Doloei, G. J. (2020). 3-D crustal structure of the Iran plateau using phase velocity ambient noise tomography. *Geophysical Journal International*, *220*(3), 1555–1568. <https://doi.org/10.1093/gji/egg257>
- Núñez, D., Córdoba, D., & Kissling, E. (2019). Seismic structure of the crust in the western Dominican Republic. *Tectonophysics*, *773*, 228224. <https://doi.org/10.1016/j.tecto.2019.228224>
- Paul, H., Singh, B., & Mandal, P. (2024). 3D shear-wave velocity structure of the Eastern Indian Shield from ambient noise tomography: Ultrafast lower crust underneath the Singhbhum Craton. *Journal of Asian Earth Sciences*, *260*, 105954. <https://doi.org/10.1016/j.jseas.2023.105954>
- Pindell, J., Kennan, L., Stanek, K. P., Maresch, W. V., & Draper, G. (2006). Foundations of Gulf of Mexico and Caribbean evolution: Eight controversies resolved. *Geológica Acta: an international earth science journal*, *4*(1–2), 303–341.
- Possee, D., Keir, D., Harmon, N., Rychert, C., Eakin, C., Rolandone, F., et al. (2020). Spatial variations in crustal and mantle anisotropy across the North American–Caribbean boundary on Haiti. *Journal of Geophysical Research: Solid Earth*, *125*(6), e2019JB018438. <https://doi.org/10.1029/2019jb018438>
- Possee, D., Keir, D., Harmon, N., Rychert, C., Rolandone, F., Leroy, S., et al. (2019). The tectonics and active faulting of Haiti from seismicity and tomography. *Tectonics*, *38*(3), 1138–1155. <https://doi.org/10.1029/2018tc005364>
- Pubellier, M., Vila, J. M., & Boisson, D. (1991). North Caribbean neotectonic events: The Trans-Haitian fault system. Tertiary record of an oblique transcurrent shear zone uplifted in Hispaniola. *Tectonophysics*, *194*(3), 217–236. [https://doi.org/10.1016/0040-1951\(91\)90262-q](https://doi.org/10.1016/0040-1951(91)90262-q)
- Quiros, D. A., Pulliam, J., Barman, D., Polanco Rivera, E., & Huérfano, V. (2018). Ambient noise tomography images accreted terranes and igneous provinces in Hispaniola and Puerto Rico. *Geophysical Research Letters*, *45*(22), 12–293. <https://doi.org/10.1029/2018gl080095>
- Rabade, S., Lin, F. C., Tape, C., Ward, K. M., Waldien, T., & Allam, A. (2023). The crustal magmatic structure beneath the Denali Volcanic Gap imaged by a dense linear seismic array. *Journal of Geophysical Research: Solid Earth*, *128*(12), e2023JB027152. <https://doi.org/10.1029/2023jb027152>
- Ramos, J. P., & Mann, P. (2023). Late Cretaceous–recent tectonostratigraphic evolution of the Yucatan back-arc basin, northern Caribbean Sea. *Geochemistry, Geophysics, Geosystems*, *24*(8), e2023GC010933. <https://doi.org/10.1029/2023gc010933>
- Saint Fleur, N., Feuillet, N., & Klinger, Y. (2019). Active tectonics along the Cul-de-Sac–Enriquillo plain and seismic hazard for Port-au-Prince, Haiti. *Tectonophysics*, *771*, 228235. <https://doi.org/10.1016/j.tecto.2019.228235>

- Shapiro, N. M., & Ritzwoller, M. H. (2002). Monte-Carlo inversion for a global shear-velocity model of the crust and upper mantle. *Geophysical Journal International*, *151*(1), 88–105. <https://doi.org/10.1046/j.1365-246x.2002.01742.x>
- Sun, L., Mann, P., & Bird, D. E. (2021). Integration of tectonic geomorphology and crustal structure across the active obliquely collisional zone on the island of Hispaniola, northeastern Caribbean.
- ten Brink, U., & Lin, J. (2004). Stress interaction between subduction earthquakes and forearc strike-slip faults: Modeling and application to the northern Caribbean plate boundary. *Journal of Geophysical Research*, *109*(B12). <https://doi.org/10.1029/2004jb003031>
- ten Brink, U. S., Bakun, W. H., & Flores, C. H. (2011). Historical perspective on seismic hazard to Hispaniola and the northeast Caribbean region. *Journal of Geophysical Research*, *116*(B12), B12318. <https://doi.org/10.1029/2011jb008497>
- Wang, Y., Lin, F. C., Schmandt, B., & Farrell, J. (2017). Ambient noise tomography across Mount St. Helens using a dense seismic array. *Journal of Geophysical Research: Solid Earth*, *122*(6), 4492–4508. <https://doi.org/10.1002/2016jb013769>
- Ward, K. M. (2015). Ambient noise tomography across the southern Alaskan Cordillera. *Geophysical Research Letters*, *42*(9), 3218–3227. <https://doi.org/10.1002/2015gl063613>
- Yang, Y., Ritzwoller, M. H., & Jones, C. H. (2011). Crustal structure determined from ambient noise tomography near the magmatic centers of the Coso region, southeastern California. *Geochemistry, Geophysics, Geosystems*, *12*(2). <https://doi.org/10.1029/2010gc003362>